Transport of Strongly Correlated Bosons in an Optical Lattice

Arya Dhar, Christian Baals, Bodhaditya Santra, Andreas Müllers, Ralf Labouvie, Thomas Mertz, Ivana Vasic, Agnieszka Cichy, Herwig Ott, and Walter Hofstetter*

The transport of strongly correlated bosons in a three-dimensional optical lattice is studied within the Bose–Hubbard approximation. The transport is induced by a small displacement of the overall harmonic trapping potential. The subsequent relaxation dynamics is monitored by high precision density measurements with the help of scanning electron microscopy. Good agreement with a real space time-dependent Gutzwiller mean-field description is found.

1. Introduction

Transport properties are among the most characteristic features of materials. Understanding and engineering the transport of mass, charge, spin, or heat opens the door for the development of new devices with new functionality. For strongly correlated materials, transport properties are especially difficult to describe, yet, their understanding is mandatory to fully exploit their application potential. Model systems, such as ultracold quantum gases, are a class of tunable systems, which contain essential aspects of real materials but are still conceptually simple enough to be amenable to advanced theoretical modeling from first principles, thus enabling quantum simulations of strongly correlated condensed matter systems.[1] They are therefore ideal candidates to understand the connection between microscopic interaction mechanisms and global transport properties.

Ultracold quantum gases have often been studied in the context of being the ground state of a many-body Hamiltonian.[2] In recent years, however, increasing interest is focused on non-equilibrium dynamics, especially with respect to transport processes.[3,4] A paradigmatic class of quantum gases are lattice gases, where the particles are residing and moving in a periodic potential, created by interfering laser beams. Optical lattices allow for easy control of the tunneling and interaction parameters, thus tuning the correlations in the system. At the same time, the system can be mapped onto seminal model hamiltonians such as the Hubbard and the Bose-Hubbard model.[5] The superfluid to Mott-insulator transition of a bosonic gas[6] is a good example how microscopic interaction and hopping mechanisms determine the quantum phases in the lattice. Similarly, the interplay between onsite correlations and hopping, and the resulting metal to Mott-insulator transition has been realized and studied with interacting spin-1/2 fermions in an optical lattice.[7,8]

Transport processes in optical lattices have a long tradition in the research of ultracold quantum gases.[9] In order to directly measure transport in optical lattices, two experimental schemes have been developed: the motion of the particles under the influence of a constant force and the motion of a trapped atomic gas after a displacement. In the first case, the generic dynamics are Bloch oscillations,[10,11] whose contrast is strongly affected by the

Dr. A. Dhar, T. Mertz, Prof. W. Hofstetter
Institut für Theoretische Physik, Max-von-Laue Str. 1
Goethe Universität
60438 Frankfurt am Main, Germany

Dr. A. Dhar
Institut für Theoretische Physik
Appelstr. 2
Leibniz Universität
30167 Hannover, Germany

C. Baals, Dr. B. Santra, Dr. A. Müllers, Dr. R. Labouvie
Department of Physics and Research Center OPTIMAS
Erwin-Schrödinger-Straße 46
Technische Universität Kaiserslautern
67663 Kaiserslautern, Germany
E-mail: ott@physik.uni-kl.de

C. Baals, Prof. H. Ott
Graduate School Materials Science in Mainz
Staudinger Weg 9, 55128 Mainz, Germany

DOI: 10.1002/pssb.201800752

Dr. B. Santra
Institut für Experimentalphysik und Zentrum für Quantenphysik
Universität Innsbruck
6020 Innsbruck, Austria

Prof. I. Vasic
Scientific Computing Laboratory
Center for the Study of Complex Systems
Institute of Physics Belgrade
University of Belgrade
11080 Belgrade, Serbia

Dr. A. Cichy
Faculty of Physics
Adam Mickiewicz University
ul. Umultowska 85, PL-61-614 Poznań, Poland

Dr. A. Cichy
Institut für Physik
Johannes Gutenberg-Universität Mainz
Staudingerweg 9, D-55099 Mainz, Germany

© 2019 WILEY-VCH Verlag GmbH & Co. KGaA, Weinheim

presence of interactions with the same species or collisions with another species.[12] The dipolar oscillation in a displaced trap[9,13,14] is conceptually related to Bloch oscillation, as the physical displacement of a parabolic trap can be described by the application of a constant force. However, the inhomogeneity of the system effectively emulates a varying local force on the atoms.

Within the Bose-Hubbard model, the generic expected phenomenology is straightforward: below the quantum phase transition to the Mott-insulator, the system is superfluid, while for a Mott-insulator, transport should be essentially blocked. Thus, in a trap displacement experiment, one expects an oscillation of the whole cloud in the superfluid phase and the absence of motion in the insulating regime. This simple phenomenology is spoiled by several effects: the first is the inhomogeneity of the system. In local density approximation, this leads to a spatially varying chemical potential and the gas develops a shell structure.[15] Superfluid motion is therefore never fully suppressed. Moreover, the finite temperature, particle hole excitations and the finite system size allow for a finite mobility even in the Mott-insulating phase.[16] The overall motion of the gas in the Mott-insulating phase is therefore nontrivial and its theoretical description requires modeling and simulating the real-space density distribution.

This was addressed in an early theoretical study,[17] where interacting bosons in one- and two-dimensional optical lattices were subject to a instantaneous displacement of a harmonic confining trap, and the resulting dynamics of the many-body system was investigated by time-dependent Gutzwiller theory. While for weak interactions damped Bloch-type oscillations were found, strong repulsive onsite interactions in 1d lead to the formation of a Mott-insulator and complete blockade of the dynamics. In two spatial dimensions, on the other hand, at longer times a "melting" of the displaced Mott-insulator was observed and, depending on the lattice geometry, also thermalization toward an equilibrium state in the shifted trap.

The above considerations motivate a precision comparison between experiment and theory, which allows to benchmark theoretical models and simulation techniques, and to understand in more detail, for example, to which extent correlations between lattice sites have to be considered to describe the system dynamics. Earlier works have primarily focussed on the transport of weakly and strongly interacting atoms in one-dimensional systems,[9,13,14] where powerful numerical tools are available.[14] The experimental signature of the transport was deduced from time of flight imaging. However, to the best of our knowledge, the effects of interaction on the transport of bosonic atoms in a three-dimensional optical lattice has not been studied in detail with high precision both from an experimental and numerical perspective.

In this work, we combine powerful experimental and numerical in situ techniques to study the center of mass motion of a bosonic quantum gas in a three-dimensional optical lattice. Displacing the overall harmonic confinement by a small amount, we induce the dynamics. By a high precision density measurement, we monitor the density distribution with high spatial resolution. Varying the lattice depth, we map out the transport through the superfluid to Mott-insulator transition. Slicing the cloud into different parts, we can also compare the inner part of the cloud with the edges. The experimental results are compared to time dependent mean-field calculations within the Gutzwiller ansatz. This method has been widely used to study time-dependent bosonic lattice problems, such as the creation of molecular Bose-Einstein condensate by dynamically melting a Mott-insulator,[18] many-body dynamics after a sudden shift of the harmonic trap,[17] creation of exotic condensates via quantum-phase-revival dynamics,[19] the Higgs-amplitude mode of strongly correlated lattice bosons,[20] collective modes of a harmonically trapped, strongly interacting Bose gas in an optical lattice,[21] quantum dynamics of interacting bosons in a three-dimensional disordered optical lattice,[22] and many more.[23–32] We also present results from a projection operator approach[33,34] with a finite energy cut-off, which we find to agree well with the Gutzwiller ansatz for our parameters.

2. Experimental Setup and Theoretical Model

The experimental sequence starts by preparing a Bose-Einstein condensate of ^{87}Rb atoms in an optical dipole trap, formed by a single beam CO_2 laser.[35] The atomic gas is cigar-shaped and the axial trap oscillation frequency is 10 Hz, while the two transverse oscillations frequencies are 145 Hz in the horizontal and 80 Hz in the vertical direction, respectively. The latter is reduced due to the gravitational sag. We then adiabatically switch on an anisotropic three-dimensional optical lattice, whose depths can be tuned individually in all three directions. After a short settling time, the dipole trap is shifted in the horizontal direction within 2 ms by about 1 μm with the help of a piezo actuated mirror, thus forcing the system out of equilibrium, (see **Figure 1**). The subsequent relaxation dynamics is imaged with the help of scanning electron microscopy (SEM)[36,37] for evolution times up to 150 ms. During the imaging procedure, the dynamics of the atomic cloud is frozen out in the optical lattice by increasing its strength to a value where tunneling is suppressed. From the SEM image of the atomic cloud, the size and the center- of-mass of the cloud are determined (**Figure 2**). Furthermore, the images are dissected into different slices for a detailed spatially resolved analysis of the mass transport. The optical lattice has a tetragonal symmetry with a lattice spacing of $d_z = 547$ nm in the axial direction and $d_x = d_y = 387$ nm in the two transverse directions. Due to geometrical constraints of the experimental setup, the orientation of the two transverse lattice axes is rotated by 45 degrees with respect to the vertical and horizontal direction.

The lattice depth is expressed in units of the recoil energy, $E = \hbar^2 k^2/(2m)$, where $k = \pi/d$ is the lattice vector and m is the mass of the atoms. As there are two different lattice constants in

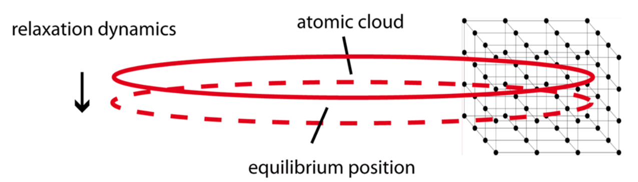

Figure 1. Setup. A cloud of ultracold bosons residing in a parabolic trap with superimposed three-dimensional optical lattice is shifted out of its equilibrium position. The subsequent relaxation dynamics is studied with high precision density measurements. The sketched optical lattice on the right side of the gas extends homogeneously over the whole cloud.

© 2019 WILEY-VCH Verlag GmbH & Co. KGaA, Weinheim

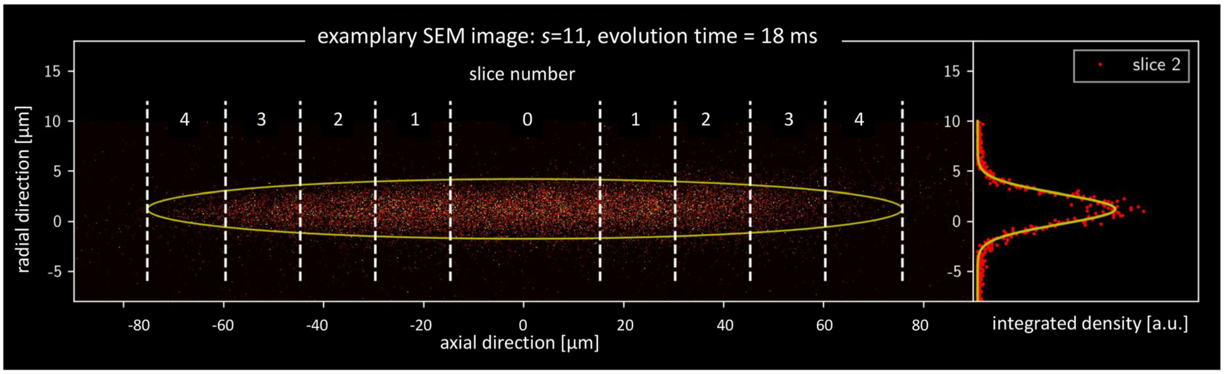

Figure 2. Scanning electron microscopy image of the BEC for $s = 11$. From Gaussian fits to the density distribution, we extract the center-of-mass of the cloud. For a more detailed analysis, we additionally slice the cloud into different segments and analyze the slices individually. Exemplary, on the right panel, we plot the radial atomic density for the second slice.

the present setup, we define individual dimensionless lattice depths,

$$s_a = \frac{V_a}{E_a} \tag{1}$$

where the index $a = x, y, z$ denotes the corresponding lattice height V_a and recoil energy E_a. The values of s_a control the ratio of the interaction energy to the tunneling amplitude, giving rise to the different quantum phases of a Mott-insulator and a superfluid.

The experimental system can be suitably described by the Bose-Hubbard model in the lowest band approximation

$$H = -\sum_{\langle i,j\rangle} J_{ij}\left(\hat{b}_i^\dagger \hat{b}_j + h.c.\right) + \frac{U}{2}\sum_i \hat{n}_i(\hat{n}_i - 1) + \sum_i (\varepsilon_i - \mu)\hat{n}_i \tag{2}$$

where $\hat{b}_i^\dagger \left(\hat{b}_i\right)$ creates (annihilates) a bosonic particle at site i, $\hat{n}_i$ is the number operator at site i, J_{ij} denotes the tunneling amplitude between nearest neighboring sites $\langle i, j\rangle$ arising from the different lattice constants along the three directions forming the optical lattice, U is the onsite interaction energy, ε_i is the potential energy at site i and μ is the chemical potential.

The tunneling couplings J_{ij} can take two different values, depending whether the particle moves along the transverse x- or y-direction ($J_x = J_y$), or along the z-direction (J_z). Within the tight binding approximation, the tunneling couplings J_a can be related to the lattice parameter with the following approximative expression,[38] valid for each lattice axis:

$$J_a \approx \frac{4}{\sqrt{\pi}} {s_a}^{3/4} E_a e^{-2\sqrt{s_a}}, \qquad a = x, y, z. \tag{3}$$

The interaction energy for a tetragonal lattice reads[2]

$$U \approx \sqrt{\frac{8}{\pi}} s^{3/4} k_l a E_r \tag{4}$$

where s, k_l, and E_r are the geometric means of the individual lattice directions. More precise values of the tunneling energy and the interaction energy can be retrieved by a band structure calculation, which we have used in this work. The values of U/J addressed in this work ranges from 0.60 to 8.21, where $J = 2\left(J_x + J_y + J_z\right)$.

To numerically study the relaxation dynamics after the shift of the dipole trap center, we use the time-dependent Gutzwiller mean-field approach, which is a well-established method, especially for higher dimensional systems.[39,40] We first calculate the ground state density distribution at $T = 0$ for the given experimental parameters (see **Figure 3**). We then time evolve the system in the shifted trapping potential. To verify the results obtained from this approach at higher values of the interaction strengths, we retained first-order corrections due to correlations within the realm of the projection operator approach and compared the results obtained from both approaches.

To obtain the ground state, we use the time independent Gutzwiller variational ansatz

$$|\psi_{GW}\rangle = \prod_{\otimes l}\sum_n c_n^{(l)} |n\rangle_l \tag{5}$$

where l denotes the site index and $|n\rangle$ denotes the Fock occupation basis. The Gutzwiller state becomes exact in the limit of large and small interactions. In order to find the ground state, we minimize the energy functional of the full Hamiltonian with respect to this state.

$$E = \frac{\langle \psi_{GW}|\hat{H}|\psi_{GW}\rangle}{\langle \psi_{GW}|\psi_{GW}\rangle} \tag{6}$$

This effectively reduces to a minimization with respect to the coefficients, $c_n^{(l)}$.

After computing the ground state, we proceed to study the time dependence by considering the coefficients in the Gutzwiller state as time dependent, that is, $c_n^{(l)}(t)$.

By applying the time-dependent variational principle, we obtain the equations of motion for all of the coefficients,

© 2019 WILEY-VCH Verlag GmbH & Co. KGaA, Weinheim

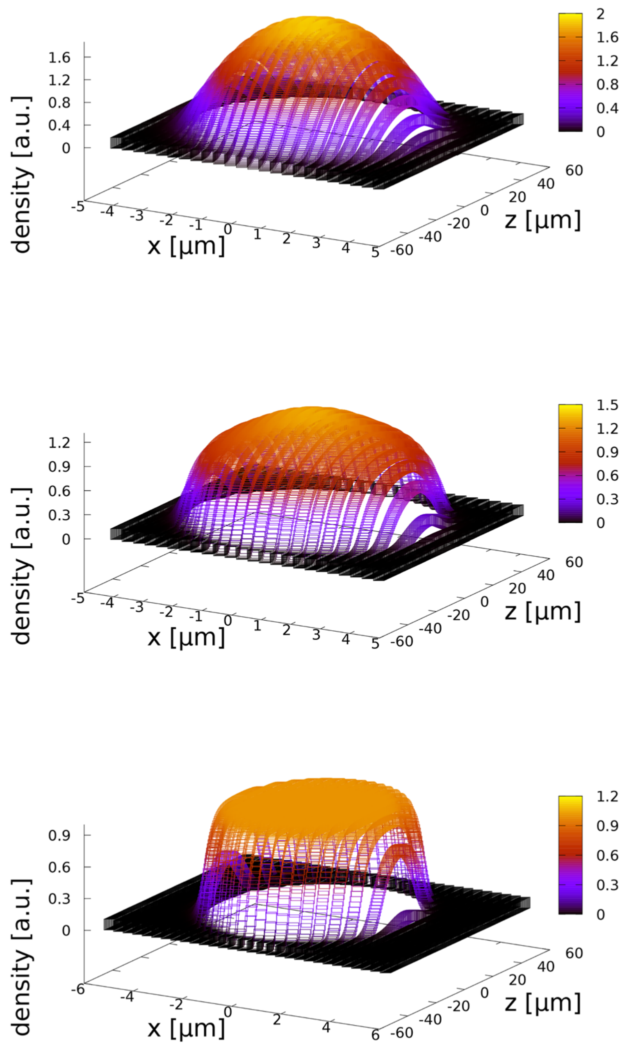

Figure 3. The ground state density distribution in the $y = 0$ plane for three values of $s = 7$ (top), 13 (middle), 16 (bottom) as simulated using Gutzwiller approximation. The density is given in atoms per lattice site.

$$
\begin{aligned}
i\partial_t c_n^{(l)} = &-J_{l,l'}\sum_{l'}\left[c_{n-1}^{(l)}\sqrt{n}\phi_{l'} + c_{n+1}^{(l)}\sqrt{n+1}\phi_{l'}^*\right] \\
&-\left[\mu n - \frac{U}{2}n(n-1) - \varepsilon_i n\right]c_n^{(l)}
\end{aligned}
\tag{7}
$$

where the sum over l' goes over all the nearest neighboring sites to l, and $\phi_l = \langle a_l \rangle$ is the condensate fraction at site l. The above equation corresponds to a set of $N_c \times L$ first order coupled differential equations, where N_c is the size of the local Hilbert space and L is the total number of sites.

To analyze the dynamics of the Bose-Hubbard model beyond mean-field theory, we have also implemented the projection operator approach.[33,34,41] This method uses a canonical transformation such that it systematically eliminates hopping processes which connect states with a large energy difference. This energy cut-off is typically chosen as the onsite interaction energy U. This will generate an effective low-energy Hamiltonian for the system in the strongly interacting limit. It should be noted that choosing this energy cut-off as infinity leads to the Gutzwiller mean-field approximation. The projection operator method gives improved phase boundaries for the superfluid to Mott-insulator transition, which are very close to the numerically exact Monte Carlo data in three spatial dimensions.[33]

To understand the projection operator approach, let us first divide our model Hamiltonian into two parts, one containing the interaction and one-body terms, and the other having the kinetic energy part:

$$
H = H_0 + \sum_{\langle ij \rangle} T_{ij} \tag{8}
$$

where $H_0 = \frac{U}{2}\sum_i \hat{n}_i(\hat{n}_i - 1) - \mu\hat{n}_i + \varepsilon_i\hat{n}_i$, and $T_{ij} = -J_{ij}\hat{b}_i^\dagger\hat{b}_j$ is the anisotropic hopping rate. The kinetic energy can be written as $T_{ij} = \sum_\beta T_{ij}$, where

$$
T_{ij}^\beta = -J_{ij}\sum_n g_\beta^n |n+1\rangle_i |n-\beta\rangle_j {}_i\langle n|_j\langle n-\beta+1| \tag{9}
$$

where $g_\beta^n = \sqrt{(n+1)(n-\beta+1)}$. T_{ij}^β connects local states differing in energy by $\varepsilon_{ij}^\beta = \beta U + \varepsilon_i - \varepsilon_j$, where $\beta = 0, \pm 1, \pm 2 \ldots$. Let us now introduce an energy scale, ΔE such that we consider a hopping process to be a low-energy process if $\left|\varepsilon_{ij}^\beta\right| < \Delta E$. For each bond $\langle ij \rangle$, we introduce a set $\beta_{ij} : \beta \in \beta_{ij}$ if the above condition is satisfied for the low energy process.

We improve the variational ansatz to

$$
|\psi(t)\rangle = e^{-i\mathscr{S}(t)}|\psi_{GW}\rangle \tag{10}
$$

where $\psi_{GW}\rangle = \prod_l \sum_n c_n^{(l)}(t)|n\rangle_l$ is the Gutzwiller wave function, and the canonical transformation, $\mathscr{S}$ introduces correlations between different lattice sites. The operator $\mathscr{S}$ is defined in such a way that higher order hopping terms in H^*, as defined below, are systematically removed up to the order $J(J//U)^{m-1}$,

$$
H^* = \exp(i\mathscr{S})H\exp(-i\mathscr{S}). \tag{11}
$$

We limit ourselves to the leading approximation $m = 1$,

$$
\mathscr{S} \approx -i\sum_{\langle ij \rangle}\sum_{\beta \notin \beta_{ij}} \frac{T_{ij}^\beta}{\varepsilon_{ij}^\beta} \tag{12}
$$

The energy cut-off is set as U. From the time dependent variational principle, we obtain improved equations of motion for the coefficients $c_n^{(l)}(t)$.[41]

3. Results

We first analyze the motion of the whole cloud during the relaxation process. The results are summarized in **Figure 4**, where the center-of-mass dynamics of the entire cloud after the sudden shift of the dipole trap center is plotted for different values of $s = s_x = s_y = 1.25 s_z$. Figure 4 constitutes the main

 © 2019 WILEY-VCH Verlag GmbH & Co. KGaA, Weinheim

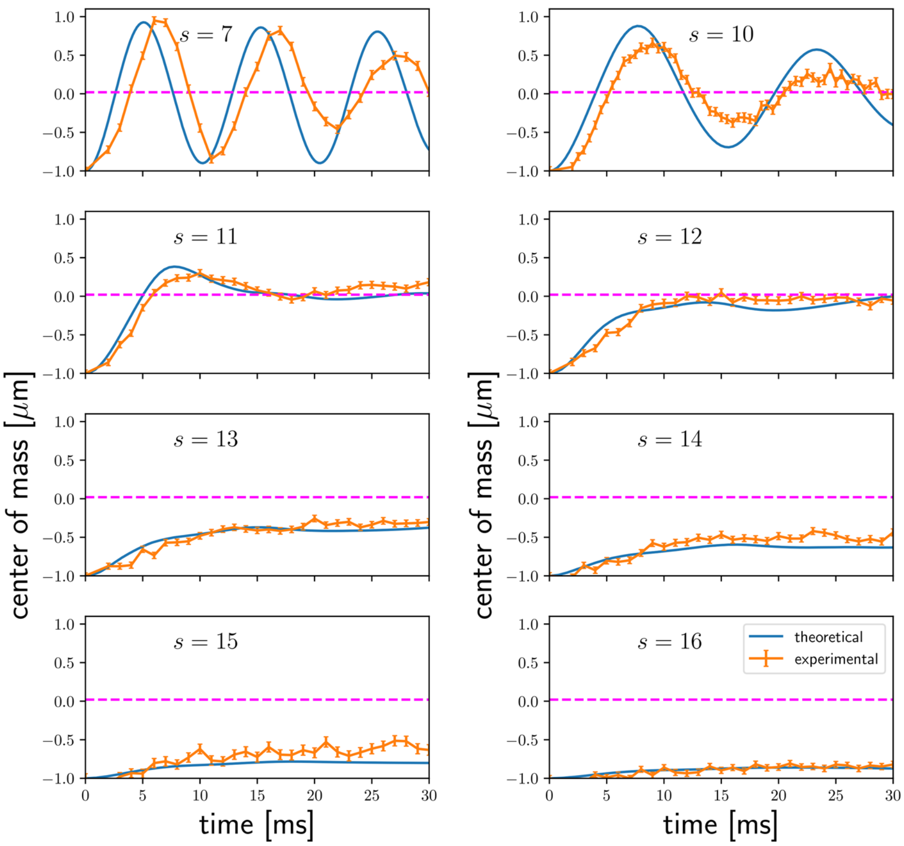

Figure 4. Time evolution of the center-of-mass after the harmonic trapping potential center is suddenly shifted. The experiment has been performed for different values of the lattice strength *s* as indicated in each of the subplots. Experimental data are shown in orange, the numerical simulation using time dependent Gutzwiller approximation is shown in blue. The magenta dashed line shows the position of the equilibrium position.

result of this work. An immediate look at the figure reveals the remarkable agreement obtained between the experimental and theoretical results for all the s values which have been considered.

We now discuss some important features of the time evolution as shown in Figure 4. For small values of s, there are large oscillations of the center-of-mass around the new trap center, shown by both theoretical and experimental results. These oscillations can be attributed to the dipolar oscillations set in by the sudden shift in the trap center.

The large amplitude of the oscillations can be traced back to the superfluid ground state covering the entire cloud. As the cloud is shifted by only two lattice sites, the whole cloud remains in the lowest band upon the displacement. The amplitude of the oscillations as obtained through the numerical simulations is found to be slightly more than that observed in the experiment. This can be due to the finite temperature effect in the experiments, which decreases the condensate fraction in the cloud, and introduces thermal fraction. On the contrary, the numerical simulations are carried out at zero temperature with the entire cloud being in the superfluid phase. The frequency difference of about 10 percent, which is visible for $s = 7$ and $s = 10$, is most likely due to a long term drift of the dipole trapping potential between the initial calibration measurement and the actual experimental runs.

More interesting features in the dynamics appear for increasing lattice depth. The relaxation dynamics is not only slowed down by the decreasing tunneling coupling, the results change also qualitatively. Already for $s = 11$, there are practically no oscillations sustained for longer times. The center-of-mass overshoots the new trap center, but then slowly converges to the equilibrium value. We attribute the absence of oscillations to the interplay between the interaction and closed single particle orbits, which are due to the fact that the bandwidth is smaller than the chemical potential. Going from $s = 12$ to $s = 13$ shows a remarkable difference in the initial dynamics of the center-of-mass of the cloud. The system displays the initial fast movement for both the s values. For $s = 12$, it reaches the equilibrium value, whereas for $s = 13$, even for longer timescales, a small offset remains (see **Figure 5**, where we show the experimental data for a 5 times longer times scale).

Hereafter the system movement becomes significantly slower. For larger s values, the center-of-mass is not able to reach the new trap center in the timescales observed in the experiment. This is caused by the decrease of the condensate fraction and rise in the Mott-insulating region in the cloud, which prohibits the transport of the bosonic atoms. Higher values of s correspond to higher interaction strengths between the atoms, leading to localized wavefunctions describing them. For $s = 16$, the movement of the entire cloud is practically negligible compared

© 2019 WILEY-VCH Verlag GmbH & Co. KGaA, Weinheim

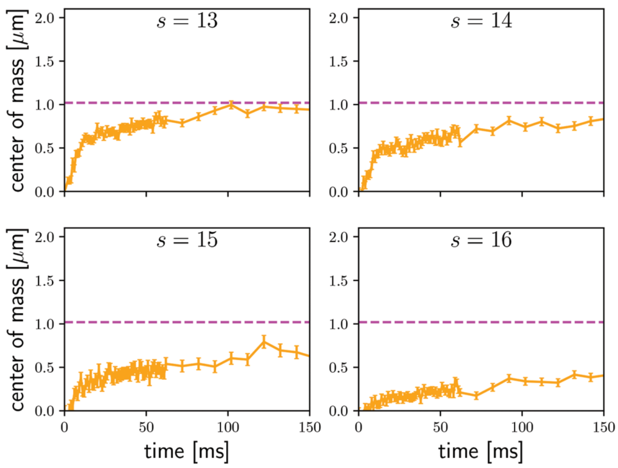

Figure 5. COM dynamics for longer times as observed in the experiment for higher values of s.

to the shift due to presence of the incompressible Mott-insulating region encompassing a vast region of the cloud.

To confirm our results, we looked at the ground state density distribution for the extreme values of s from the numerical simulations using Gutzwiller approximation and indeed, we find the superfluid and Mott-insulating phases in the cloud as shown in Figure 3. It shows the existence of superfluid phase in the entire cloud for $s = 7$ whereas for $s = 13$, a thin MI shell arises in the intermediate region of the cloud, and a clear density plateau for $s = 16$ implies the appearance of Mott-insulating region at the central part with superfluid wings. The simulations were carried out with typical system sizes of $25 \times 25 \times 180$ sites along x,y,z directions, respectively. The larger number of sites along the z direction, which has the weakest trapping amplitude, were taken in accordance with the experiment. The choice of chemical potential was done such that the total number of particles were $\approx$30000. Depending on the s-value, a convergence test was performed to select the appropriate occupation cut-off on a single site.

To have a deeper understanding of the movement of the atoms, we sliced the cloud in several sections as shown in Figure 2. The width of each of the slices is 100 pixels, which correspond to $\approx 15\,\mu$m. The slices are paired because of the mirror symmetry. Each slice is integrated in the axial direction to get a 1D profile, which is fitted with a Gaussian function to determine its center. The error of this center is given by the standard deviation σ from the Gaussian fit divided by $\sqrt{I}$, where I is the summed intensity of the corresponding slice.

Since the movement of the atoms is related to the superfluid nature of the atomic cloud, it is instructive to first look at the condensate fraction of the different parts of the cloud, defined as

$$\Phi = \sum_{i \in \mathrm{slice}} \frac{\phi_i^2}{n_i} \tag{13}$$

where $\phi_i = \langle b_i \rangle$ at site i. This quantity cannot be measured in the current experimental setup and we resort to the numerical simulations, having already established the reliability on the data obtained from time-dependent Gutzwiller method. **Figure 6** shows the condensate fraction of different slices corresponding to different values of s. For $s = 7$, we see that the entire cloud has condensate fraction close to 1. As the lattice depth increases, the condensate fraction in the inner slices decreases much faster than in the outer wings. This is a clear signature of the increasing Mott-insulating character in the inner sections of the cloud. Consequently, we expect for all lattice parameters a larger mobility of the atoms towards the edges of the cloud.

Figure 7 shows the comparison between experiment and theory for the individual slices for $s = 13$. The experimental data for all slices look very similar. A closer look reveals that the outer slices show a slightly faster motion toward the equilibrium position as compared to the inner slices. For all slices, no oscillations are visible. The theoretical simulation shows a similar trend with respect to the motion: the inner slices have a slower initial motion towards the equilibrium position. This is compatible with the onset of a Mott-insulator shell in the trap center at $s = 13$. For the outer slices, however, the simulations predict clearly visible oscillations. This is in contrast to the experimental findings. From an analysis of the numerical data, we find that the outer shells indeed host a superfluid and can therefore undergo a damped oscillation. Two reasons can be responsible for the absence of oscillations in the experiment: In the experiment, we have a finite temperature of about $T = 30$ nK. This is already sufficient to smear out the shell structure of the Mott-insulator plateaus significantly,[16] thus smearing out the dynamics of the slices. Another consequence of the finite temperature is the appearance of a normal (thermal) component at the edges of the cloud, which is not undergoing superfluid behavior. The appearance of a thermal component goes along with a depletion of the superfluid fraction. Note that the bandwidth of the optical lattice for $s \geq 12$ is smaller than the thermal energy. This interpretation is compatible with the fact that the overall center-of-mass motion shows very good agreement, indicating the presence of an effective smearing out taking place in the experiment. A comparison of the individual slices for a lattice depth of $s = 16$ shown in **Figure 8** shows qualitatively similar results. Again, the outer slices show

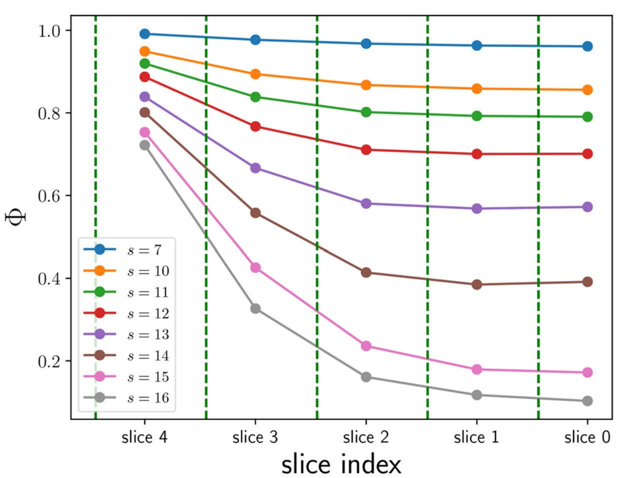

Figure 6. Ground state condensate fraction, explained in the text, for different slices marked by green dashed lines for various s values.

© 2019 WILEY-VCH Verlag GmbH & Co. KGaA, Weinheim

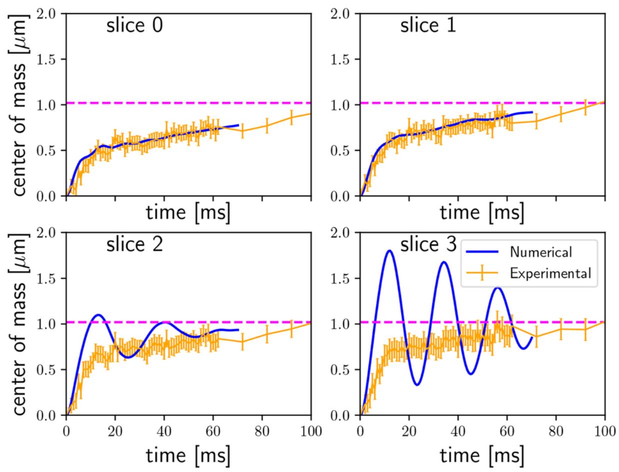

Figure 7. Comparison of the center-of-mass dynamics for different slices from the experiment (orange) and numerical simulations (blue) for $s = 13$. The slices are defined in Figure 2.

residual oscillations. Note that these oscillations persist, even though the cloud is well in the Mott-insulating regime. In addition to the above two reasons, one should also take into account the fact that the Gutzwiller approximation overestimates the condensate fraction, as discussed in ref. [33]. This can also contribute to the discrepancy between the theory and experimental results for the motion of the outer slices.

The results obtained from the time-dependent Gutzwiller method ignores quantum correlations between the different lattice sites. We implement an independent method based on the projection operator approach to include additional quantum correlations. The main motivation for this endeavour is to investigate the validity of the approximation in the Gutzwiller method. As discussed before, the projection operator approach with an infinite energy cut-off reduces to the Gutzwiller mean-field theory. Keeping a finite energy cut-off equal to the corresponding U, we can thus include hopping processes which

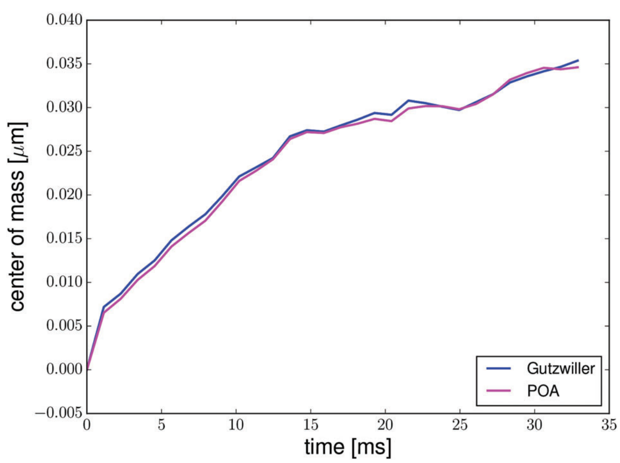

Figure 8. Comparison of the center-of-mass dynamics for different slices from the experiment (orange) and numerical simulations (blue) for $s = 16$. The slices are defined in Figure 2.

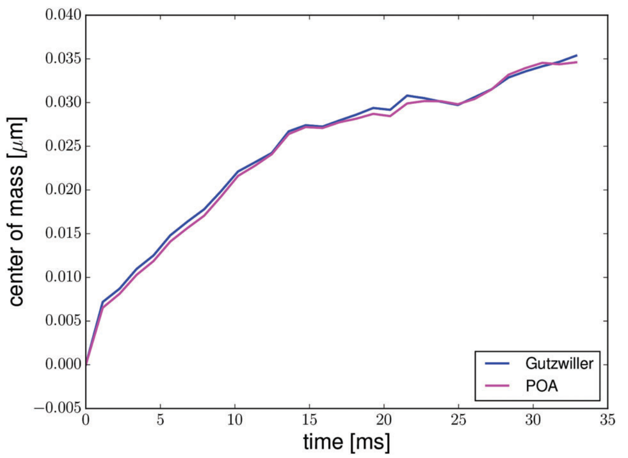

Figure 9. COM dynamics for a smaller system size obtained from time-dependent Gutzwiller (blue) and the projection operator approach method (magenta).

do not change the energy more than the energy cut-off, thus retaining quantum correlations with neighboring sites. However, for the projection operator approach, we are limited by smaller system sizes. **Figure 9** shows the COM dynamics for a smaller system size ($12 \times 12 \times 14$ along $x - y - z$) for $s = 16$ obtained from time-dependent Gutzwiller projection operator approach method. Indeed they show remarkable agreement for timescales studied in this work. This result thus confirms the validity of the Gutzwiller approximation in this parameter regime.

4. Conclusions

We have studied transport of interacting bosons in an optical lattice, for a range of interaction strengths across the superfluid to Mott-insulator quantum phase transition, by using a high resolution scanning electron microscopy technique. We have clearly observed dipolar oscillations in the superfluid regime, whereas in the presence of a pronounced Mott-plateau the system showed a strongly suppressed mobility due to suppressed tunneling. We compared our experimental findings to simulations based on time-dependent Gutzwiller theory, and found very good agreement. For smaller system sizes, the time dependent Gutzwiller method was successfully benchmarked with the projection operator approach. Several open questions will be the subject of future research. These include the possible melting of the Mott-insulator at long time scales and the dependence of thermalization dynamics on the lattice geometry, as indicated by earlier studies.[17] Furthermore, it would be of interest to take into account by more advanced simulation techniques also the tunneling dynamics of the normal bosonic component at finite temperature.

Acknowledgement

This work was funded by the Deutsche Forschungsgemeinschaft (DFG, German Reserach Foundation), project number 31867626 (SFB/TR 49, projects A3 and A9). We further acknowledge funding by the Deutsche

© 2019 WILEY-VCH Verlag GmbH & Co. KGaA, Weinheim

Forschungsgemeinschaft (DFG, German Reserach Foundation), project number 277625399 (SFB/TR 185) and project number 49741853 (Graduate School of excellence MAINZ). The research was also funded and by the state of Rhineland-Palatinate within the research center OPTIMAS and by the National Science Centre (NCN, Poland) under grant: UMO-2017/24/C/ST3/00357 (A.C.). I.V. acknowledges support by the Ministry of Education, Science, and Technological Development of the Republic of Serbia under Projects ON171017 and BKMH, and by DAAD (German Academic and Exchange Service) under the BKMH project.

Conflict of Interest

The authors declare no conflict of interest.

Keywords

bosonic Mott insulator, Gutzwiller approach, transport, ultracold quantum gases

Final Version: March 15, 2019
Received: December 21, 2018
Published online: April 15, 2019

[1] W. Hofstetter, T. Qin, *J. At. Mol. Phys*. **2018**, *51*, 082001.
[2] I. Bloch, J. Dalibard, W. Z. Werger, *Rev. Mod. Phys*. **2008**, *80*, 885.
[3] T. Kinoshita, T. Wenger, D. S. Weiss, *Science* **2004**, *305*, 1125.
[4] J. P. Brantut, J. Meineke, D. Stadler, S. Krinner, T. Esslinger, *Science* **2012**, *337*, 1069.
[5] I. Bloch, J. Dalibard, S. Nascimbène, *Nature Phys*. **2012**, *8*, 267.
[6] M. Greiner, O. Mandel, T. Esslinger, T. W. Hänsch, I. Bloch, *Nature* **2002**, *415*, 39.
[7] U. Schneider, L. Hackermüller, S. Will, T. Best, I. Bloch, T. Costi, R. Helmes, D. Rasch, A. Rosch, *Science* **2008**, *322*, 1520.
[8] R. Jördens, N. Strohmaier, K. Günter, H. Moritz, T. Esslinger, *Nature* **2008**, *455*, 204.
[9] F. S. Cataliotti, S. Burger, C. Fort, P. Maddaloni, F. Minardi, A. Trombettoni, A. Smerzi, M. Inguscio, *Science* **2001**, *293*, 843.
[10] M. Ben Dahan, E. Peik, J. Reichel, Y. Castin, C. Salomon, *Phys. Rev. Lett*. **1996**, *76*, 4508.
[11] G. Roati, E. de Mirandes, F. Ferlaino, H. Ott, G. Modugno, M. Inguscio, *Phys. Rev. Lett*. **2004**, *92*, 230402.
[12] H. Ott, E. de Mirandes, F. Ferlaino, G. Roati, G. Modugno, M. Inguscio, *Phys. Rev. Lett*. **2004**, *92*, 160601.
[13] C. D. Fertig, K. M. O'Hara, J. H. Huckans, S. L. Rolston, W. D. Phillips, J. V. Porto, *Phys. Rev. Lett*. **2005**, *94*, 120403.
[14] I. Danshita, C. W. Clark, *Phys. Rev. Lett*. **2009**, *102*, 030407.
[15] S. Fölling, A. Widera, T. Müller, F. Gerbier, I. Bloch, *Phys. Rev. Lett*. **2006**, *97*, 060403.
[16] F. Gerbier, *Phys. Rev. Lett*. **2007**, *99*, 120405.
[17] M. Snoek, W. Hofstetter, *Phys. Rev. A* **2007**, *76*, 051603.
[18] D. Jaksch, V. Venturi, J. I. Cirac, C. J. Williams, P. Zoller, *Phys. Rev. Lett*. **2002**, *89*, 040402.
[19] M. Buchhold, U. Bissbort, S. Will, W. Hofstetter, *Phys. Rev. A* **2011**, *84*, 023631.
[20] U. Bissbort, S. Götze, Y. Li, J. Heinze, J. S. Krauser, M. Weinberg, C. Becker, K. Sengstock, W. Hofstetter, *Phys. Rev. Lett*. **2011**, *106*, 205303.
[21] M. Snoek, *Phys. Rev. A* **2012**, *85*, 013635.
[22] P. Buonsante, L. Pezz'e, A. Smerzi, *Phys. Rev. A* **2015**, *91*, 031601.
[23] J. Wernsdorfer, M. Snoek, W. Hofstetter, *Phys. Rev. A* **2010**, *81*, 043620.
[24] M. Snoek, *EPL (Europhys. Lett.)* **2011**, *95*, 30006.
[25] M. Jreissaty, J. Carrasquilla, F. A. Wolf, M. Rigol, *Phys. Rev. A* **2011**, *84*, 043610.
[26] K. V. Krutitsky, P. Navez, *Phys. Rev. A* **2011**, *84*, 033602.
[27] J. S. Bernier, D. Poletti, P. Barmettler, G. Roux, C. Kollath, *Phys. Rev. A* **2012**, *85*, 033641.
[28] P. Buonsante, L. Orefice, A. Smerzi, *Phys. Rev. A* **2013**, *87*, 063620.
[29] D. S. Lühmann, *Phys. Rev. A* **2013**, *87*, 043619.
[30] A. Rapp, *Phys. Rev. A* **2013**, *87*, 043611.
[31] I. Vidanović, D. Cocks, W. Hofstetter, *Phys. Rev. A* **2014**, *89*, 053614.
[32] T. Mertz, I. Vasić, M. J. Hartmann, W. Hofstetter, *Phys. Rev. A* **2016**, *94*, 013809.
[33] C. Trefzger, K. Sengupta, *Phys. Rev. Lett*. **2011**, *106*, 095702.
[34] A. Dutta, C. Trefzger, K. Sengupta, *Phys. Rev. B* **2012**, *86*, 085140.
[35] T. Gericke, P. Würtz, D. Reitz, C. Utfeld, H. Ott, *Appl. Phys. B* **2007**, *89*, 447.
[36] T. Gericke, P. Würtz, D. Reitz, T. Langen, H. Ott, *Nat. Phys*. **2008**, *4*, 949.
[37] B. Santra, H. Ott, *J. Phys. B* **2015**, *48*, 122001.
[38] W. Zwerger, *J. Opt. B: Quantum Semiclassical Opt*. **2003**, *5*, S9.
[39] W. Metzner, D. Vollhardt, *Phys. Rev. Lett*. **1989**, *62*, 324.
[40] D. S. Rokhsar, B. G. Kotliar, *Phys. Rev. B* **1991**, *44*, 10328.
[41] C. H. Lin, R. Sensarma, K. Sengupta, S. Das Sarma, *Phys. Rev. B* **2012**, *86*, 214207.

© 2019 WILEY-VCH Verlag GmbH & Co. KGaA, Weinheim